

Decalcification using ethylenediaminetetraacetic acid for clear microstructure imaging of cochlea through optical coherence tomography

Jaeyul Lee
Kanghae Kim
Ruchire Eranga Wijesinghe
Doekmin Jeon
Sang Heun Lee
Mansik Jeon
Jeong Hun Jang

Decalcification using ethylenediaminetetraacetic acid for clear microstructure imaging of cochlea through optical coherence tomography

Jaeyul Lee,^a Kanghae Kim,^a Ruchire Eranga Wijesinghe,^a Doekmin Jeon,^a Sang Heun Lee,^b Mansik Jeon,^{a,*} and Jeong Hun Jang^{c,*}

^aKyungpook National University, School of Electronics Engineering, College of IT Engineering, 80 Daehak-ro, Buk-gu, Daegu 41566, Republic of Korea

^bDaegu Veterans Hospital, Department of Otorhinolaryngology, 60 Wolgok-ro, Dalseo-gu, Daegu 42835, Republic of Korea

^cAjou University, School of Medicine, Department of Otorhinolaryngology-Head and Neck Surgery, 164 World cup-ro, Yeongtong-gu, Suwon, Gyeonggi-do 41944, Republic of Korea

Abstract. The aim of this study was to analyze the effectiveness of decalcification using ethylenediaminetetraacetic acid (EDTA) as an optical clearing method to enhance the depth visibility of internal soft tissues of cochlea. *Ex vivo* mouse and guinea pig cochlea samples were soaked in EDTA solutions for decalcification, and swept source optical coherence tomography (OCT) was used as imaging modality to monitor the decalcified samples consecutively. The monitored noninvasive cross-sectional images showed that the mouse and guinea pig cochlea samples had to be decalcified for subsequent 7 and 14 days, respectively, to obtain the optimal optical clearing results. Using this method, difficulties in imaging of internal cochlea microstructures of mice could be evaded. The obtained results verified that the depth visibility of the decalcified *ex vivo* samples was enhanced. © 2016 Society of Photo-Optical Instrumentation Engineers (SPIE) [DOI: 10.1117/1.JBO.21.8.081204]

Keywords: cochlea; decalcification; ethylenediaminetetraacetic acid; swept source optical coherence tomography.

Paper 150879SSR received Dec. 31, 2015; accepted for publication Feb. 23, 2016; published online Mar. 16, 2016.

1 Introduction

The structural integrity of cochlea is crucial for a precise auditory function. It is immensely difficult to examine the *in vivo* anatomical structure, since it is located deep within the temporal bone.¹ Hence, histopathologic studies have been commonly used to acquire the structural information on cochlea.^{2,3} These studies represent chemical fixation, dissection and embedment, and sectioning, which result in inconsistent quality and poor resolution of a histopathologic image. In addition, since these methods are invasive, these procedures should be repeated using several tissue samples to obtain an appropriate image. *In vivo* imaging modalities, such as magnetic resonance imaging and computed tomography, are noninvasive methods of evaluation of the cochlear structure. However, the resolution of these modalities is ~0.5 to 1.0 mm, which is less than the necessary resolution to detect clearly visible internal structures of the cochlea.^{4,5} Using optical coherence tomography (OCT), the real-time cross-sectional image of a microstructure can be obtained noninvasively. Therefore, OCT has been applied to visualize internal structures in the fields of ophthalmology⁶ and dermatology.⁷ In the case of OCT, internal tissue microstructures can be visualized with a resolution of 10 μm and a penetration of ~2 to 3 mm.⁸⁻¹²

The applications of OCT to otologic research, such as imaging of the cochlea, have not been reported frequently, owing to its relatively less depth penetration, middle ear location, and anatomical information.¹³⁻¹⁵ Hence, several studies have been

reported showing a very limited cochlea region in the mouse, rat, and porcine.¹⁶⁻¹⁸ Moreover, the augmentation of OCT combined with a surgical microscope method to visualize *in vivo* mouse cochlea was recently demonstrated by our group.¹⁹

Ethylenediaminetetraacetic acid (EDTA) is an aminopolycarboxylic acid. It is widely used to sequester metal ions, such as Ca^{2+} and Fe^{3+} , as a hexadentate ligand and a chelating agent. In histopathology, it is commonly used as a decalcifying agent allowing cutting of sections using a microtome when a tissue sample is demineralized.

In this study, we analyzed the efficacy of the decalcification method by soaking both *ex vivo* mouse and guinea pig cochlea samples in EDTA to obtain rigorous information on the cochlea internal microstructures.²⁰ Thus, the imaging limitations due to the mouse and guinea pig cochlea structure were overcome.²¹ Consequently, we conducted the study to confirm the required approximate soaking duration to attain the most optimal depth visibility for both mouse and guinea pig cochlea samples.²² This method emphasizes the potential to observe the entire cochlea microstructures and soft tissues, which is crucial to understand the nature of cochlear damages.

2 Methods and Materials

2.1 Cochlea Sample Preparation

The animal experiments were conducted in accordance with the guidelines of the Institutional Animal Care and Use Committee of Kyungpook National University. Five mouse cochlea samples (ICR-male mice five weeks old with masses of 25 to 30 g) were

*Address all correspondence to: Mansik Jeon, E-mail: msjeon@knu.ac.kr; Jeong Hun Jang, E-mail: jangjh@knu.ac.kr

used. Simultaneously, five guinea pig cochlea samples (Hartley albino male guinea pigs eight weeks old with masses of 310 to 340 g) were used. The animals were anesthetized using an isoflurane machine integrated anesthetic cage, and 1% of isoflurane was mixed with oxygen for the anesthetization. Prior to cochlea surgery, we performed cardiac perfusion to fix via the blood flow and preserve perfect morphology of biological tissue keeping under living condition. The animals were perfused with 30 ml of 1X phosphate buffer saline (PBS), pH 7.4, followed by 30 ml of 4% paraformaldehyde in PBS, pH 7.4. The surgery was conducted to obtain the cochlea samples, and the samples were stored in cryotubes with 1.8 ml of 4% paraformaldehyde in PBS, pH 7.4 at room temperature (24°C) (control stage) to barricade external chemical reactions. Further, the cochlea samples were soaked with 1.8 ml EDTA 10%, pH 7.4.²³ The samples were placed on a tilting shaker for decalcification (80 times/min) at room temperature, and the EDTA solution was changed every day.²⁴

2.2 Optical Coherence Tomography System Configuration

The implemented imaging modality is a commercially available swept source OCT (SS-OCT) system (Thorlabs Inc., OCS1310V1 OCT) that is centered at 1300 nm with a full width of >97 nm at half maximum of the optical spectrum and an average output power of 20 mW. The axial and transverse resolutions of the system in air are 16 and 25 μm , respectively. Further details about the system configuration can be found in Table 1.

The images were obtained on the control, 1st, 3rd, 7th, 9th, 14th, 18th, and 21st days after immersing the *ex vivo* samples in EDTA. The initial control images were obtained using 1.8 ml of 4% paraformaldehyde, 1X PBS soaked samples. The two-dimensional (2-D) images with a size of 1034 \times 610 pixels were obtained from the *ex vivo* samples. The fields of view of the mouse and guinea pig cochlea samples were $\sim 4 \text{ mm} \times 6 \text{ mm}$ and $7 \text{ mm} \times 6 \text{ mm}$, respectively. The quantitative assessment was demonstrated using an automated program (coded using MATLAB[®]) to obtain amplitude scans (A-scans) in both the axial and transverse directions for evaluating the depth enhancement in the axial direction and the thickness of the microstructures in the lateral direction.

Table 1 Specifications of the SS-OCT system.

Parameters	Specifications
Central wavelength	1300 nm \pm 15 nm
Spectral bandwidth	> 97 nm (-10 dB cut-off point)
Axial scan rate	100 kHz
Maximum imaging width	10 mm
Maximum imaging depth	> 12 mm
Transverse resolution	25 μm
Axial resolution air/water	<16 μm /12 μm

3 Results and Discussion

To evaluate the utilized 1300 nm SS-OCT system performance, we reconstructed three-dimensional (3-D) OCT images of mouse and guinea pig cochlea samples. Figures 1(a) and 1(b) show the 3-D OCT images of the entire *ex vivo* mouse and guinea pig cochlea samples as well as the photograph images [Figs. 1(c) and 1(d)]. The 3-D images were obtained from the red dashed region of the photographs. Our system provides deep structural visualization of the obtained 3-D images in the X-Y-Z axes. The overall volume of the cochlea structure can be confirmed using the acquired 3-D images. Additionally, it facilitates the analysis of structural features in various locations. Thus, a clear correlation between the photographs and the reconstructed 3-D images can be observed.

Using our SS-OCT system, first, we performed the experiment on the mouse cochlea, which was soaked in EDTA for decalcification. The image acquisition was performed on the control, 1st, 3rd, 7th, 9th, 14th, 18th, and 21st days. The obtained images are shown in Fig. 2. The cross-sectional image of the control sample is shown in Fig. 2(a) depicting the least depth visibility. Owing to the microstructural size of the mouse cochlea being smaller than that of guinea pig cochlea, the anatomical structure was decalcified rapidly, and identifiable abrupt depth visibility could be observed on the first imaging day. Continuation of the depth visibility enhancement was observed in other images according to continuation of the process. Therefore, it can be concluded that the decalcification-based optical clearing method plays a vital role for obtaining the information on the microstructural depth. Figure 2 shows that the mouse cochlea comprises a wide variety of tissue types, such as Reissner's membrane, Basilar membrane, organ of Corti, and modiolus, which can be remarkably visualized on the seventh imaging day. The aforementioned tissues are indicated using red-colored arrows.

To evaluate the proposed method precisely, the obtained images were involved in an intensity analysis to verify the deep microstructures. Thus, an automated program was coded using MATLAB[®] to analyze the pixel intensity of the

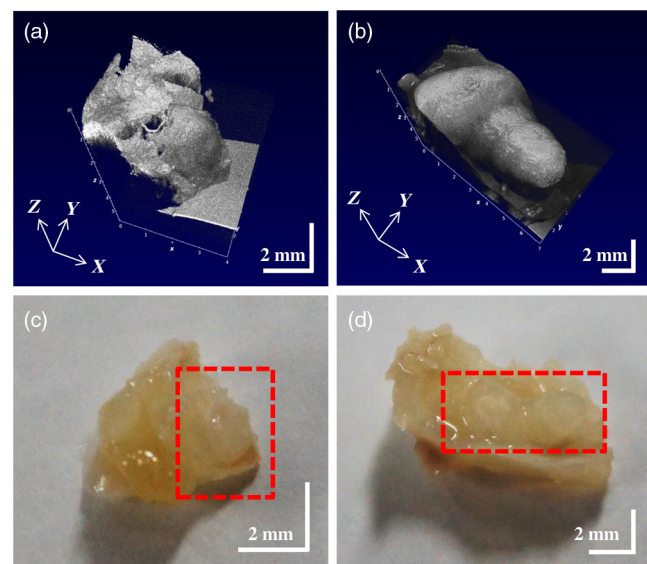


Fig. 1 Images of the cochlea samples: OCT 3-D images of (a) the mouse and (b) guinea pig cochlea samples, and photographs of (c) the mouse and (d) guinea pig cochlea samples.

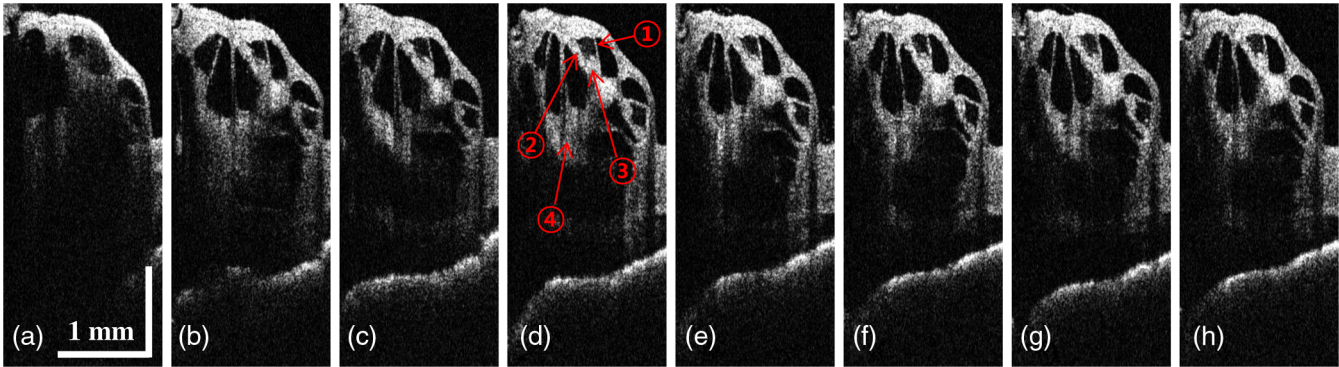


Fig. 2 2-D SS-OCT images of the mouse cochlea for detecting the depth visibility enhancement after optical clearing: (a) control sample image and (b) to (h) the experimental results obtained on the 1st, 3rd, 7th, 9th, 14th, 18th, and 21st imaging days. ①: Reissner's membrane, ②: Basilar membrane, ③: organ of Corti, and ④: modiolus.

image in the lateral directions. Demodulated raw data were loaded, and the intensities of depth direction A-scan signals were then averaged in the lateral direction. The averaged intensity is indicated in Fig. 3. Similar intensity calculation can be seen in the experimental plots within the depth range of 0 to 0.7 mm. However, compared to the control sample, a rise of the intensity can be observed in all the other plots beyond a depth of 0.7 mm, which verifies the effectiveness of decalcification. A noticeable intensity increase can be seen in the red dashed square region (the depth range of 2.8 to 3.3 mm) compared to the control sample intensity, which confirms the feasibility of the proposed clearing method. The averaged intensity values for the control stage and the seventh day were 0.06 and 0.23, respectively. Thus, the average intensity on the seventh day increased by 3.8 times compared to that for the control stage. Moreover, the overall intensity increase on each imaging day is 2.6 times (1st day), 3.6 times (3rd day), 3.8 times (7th day), 3.4 times (14th day), and 3.3 times (21st day) compared to that for the control stage. Hence, the obtained data confirm the efficacy of the EDTA-based decalcification method.

This study was an observational study, and the data analysis was primarily descriptive. A continuous variation of the laser source power was observed, which was compensated afterward. Because of the instability of the laser power, the entire intensity of the OCT images was compensated by multiplying $\pm 5\%$. Further, the entire intensity of the mouse cochlea 2-D OCT

images were summed and averaged each imaging day. The statistical parameters, such as the mean and the standard deviation, were calculated according to each specific mouse cochlea sample and averaged on each corresponding day. The results are plotted in Fig 4(a). For better understanding, a quantitative analysis was performed for further numerical evaluation. In our calculation [Fig. 4(a)], the averaged intensity of the control sample was 1.19 ± 0.11 and the maximal intensity (seventh day) was 1.95 ± 0.08 . Therefore, an intensity increase of 63.9% compared to the control sample occurs on the seventh day. Moreover, we calculated the intensity variation with respect to that for the control sample for each experimental day. The obtained values increased by 31.6% (1st day), 38.8% (3rd day), 63.9% (7th day), 63.9% (14th day), and 63.8% (21st day). The results confirm that the maximal intensity was observed on the seventh day, and further, the total intensity in the following days is saturated. Therefore, it was revealed that the most optimal duration of decalcification of the mouse cochlea was seven days.

To verify the efficacy of the proposed optical clearing method further and to confirm the enhancement of the depth intensity precisely, we analyzed the averaged intensity fluctuation of all five samples according to the imaging depth. The results are shown in Fig 4(b). Starting from a depth of 0 mm, the analysis was performed for the entire visible depth of 4 mm with a gap of 1 mm. Owing to the highest intensity, a noticeable intensity fluctuation was not observed in the depth

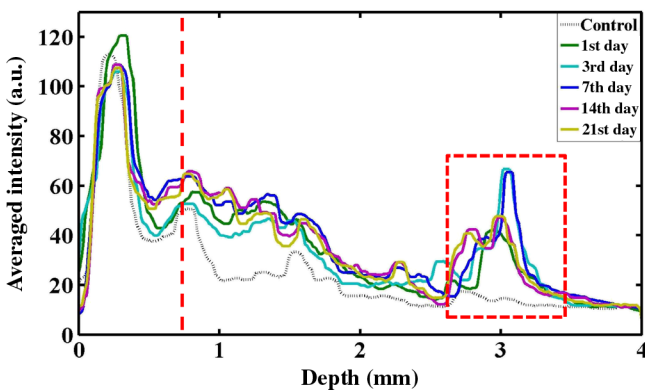


Fig. 3 Averaged intensity of the decalcified mouse cochlea OCT image in the depth direction on each imaging day.

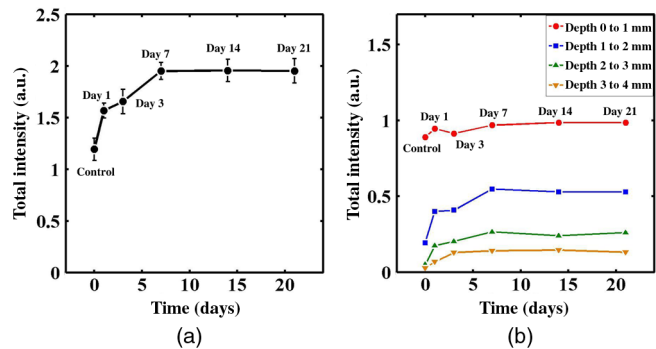


Fig. 4 Intensity analysis of the decalcified mouse cochlea OCT images: (a) the averaged intensity in the depth direction on each imaging day and (b) the total intensity with respect to the specific depth range on each imaging day.

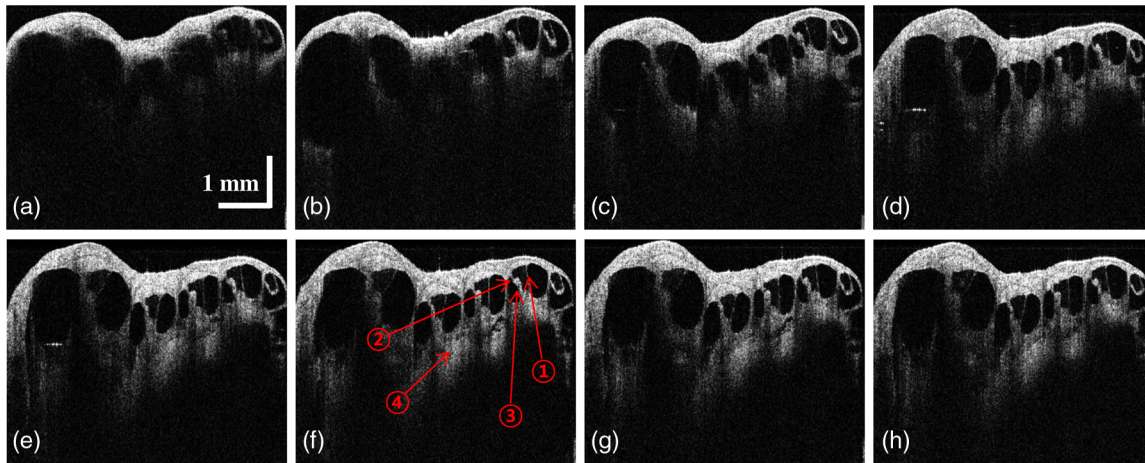


Fig. 5 2-D SS-OCT images of guinea pig cochlea for detecting the depth visibility enhancement after optical clearing: (a) the control sample image and (b) to (h) the experimental results obtained on the 1st, 3rd, 7th, 9th, 14th, 18th, and 21st imaging days. ①: Reissner's membrane, ②: Basilar membrane, ③: organ of Corti, ④: modiolus.

range of 0 to 1 mm. However, an identifiable intensity fluctuation was observed in the following depth ranges: 1 to 4 mm owing to the effects of decalcification. The intensity variation of all depth ranges shown in Fig. 4(b) was calculated by comparing the intensity fluctuation on each experimental day with that for the control stage. Therefore, fluctuations of 6.3, 2.6, 8.8, 10.8, and 10.8% were observed within the depth range of 0 to 1 mm on the 1st, 3rd, 7th, 14th, and 21st days, respectively. Simultaneously, variations of 107.1, 111.1, 183.1, 173.8, and 173.5% were observed within the depth range of 1 to 2 mm on the 1st, 3rd, 7th, 14th, and 21st days, respectively. The intensity increased by 183.1% on the seventh day compared to that for the control stage and became saturated within the following range. In the depth range of 2 to 3 mm, the intensity increased by 417.9% on the seventh day compared to that for the control stage and became saturated within $\pm 10\%$. Similarly, the intensity increased by 440.8% on the seventh day and became saturated within $\pm 10\%$ in the depth range of 3 to 4 mm.

An identical experiment was performed to visualize the *ex vivo* guinea pig cochlea samples to understand the optical clearing process better. The obtained 2-D images representing the morphological variations are illustrated in Fig. 5. Similar to the previous study, the control sample has the least depth visibility and an enhanced depth is observed in the following images according to continuation of the decalcification process. However, compared with the mouse cochlea, when the visible depth range increased abruptly, in this case, behavior of the morphological variation differed as the visible depth range increased gradually. Similar to the mouse cochlea, the guinea pig cochlea comprises a wide variety of tissue types such as Reissner's membrane, Basilar membrane, organ of Corti, and modiolus, which can be clearly visualized on the 14th day because of decalcification compared to the control sample. The aforementioned tissues are shown using red-colored arrows.

We repeated the previous intensity quantification procedures along with the optical clearing process to obtain the intensity fluctuation of the samples. Although the intensity values within the depth range of 0 to 0.5 mm are similar, those within the depth range of 0.5 to 4.3 mm are different. In particular, the result obtained on the 14th day confirms the maximum intensity

level. The obtained results are illustrated in Fig. 6. The red dashed square region of the plot depicts the gradual increase of the intensity with respect to the experimental days. In this case, a noticeable intensity increase can be observed in the red-dashed square region (1 to 3 mm depth range) compared to the control sample intensity, which confirms the feasibility of the proposed clearing method. The averaged intensity values for the control stage and on the 14th day were 0.10 and 0.52, respectively. The average intensity on the 14th day increased by 5.2 times compared to the control stage. Subsequently, compared to the control stage, an overall intensity increase of 1.4, 2.8, 4.1, 5.2, and 4.7 times on the 1st, 3rd, 7th, 14th, and 21st days, respectively, confirms the efficacy of the EDTA-based decalcification method.

Similar to the mouse cochlea study, the entire image intensity of the samples was compared and shown in Fig. 7(a). In this case, the intensity reaches up to the maximum on the 14th day and the intensity saturation can be observed on later days. Therefore, it was revealed that the most optimal duration of decalcification of the guinea pig cochlea was 14 days using the acquisition of the image with the maximal intensity. Note that the obtained intensity values were greater than that of the mouse cochlea samples, because of the size of the guinea

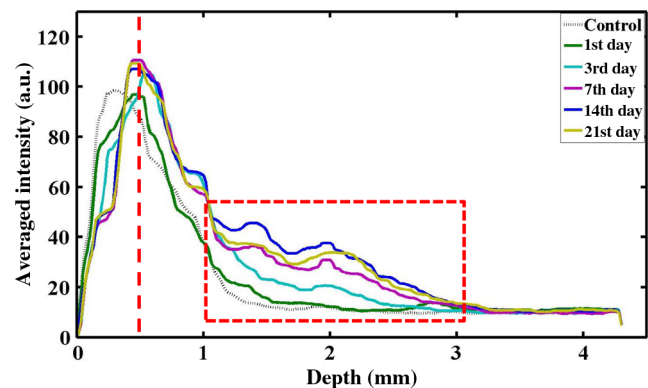


Fig. 6 Averaged intensity of the decalcified guinea pig cochlea OCT image in the depth direction on each imaging day.

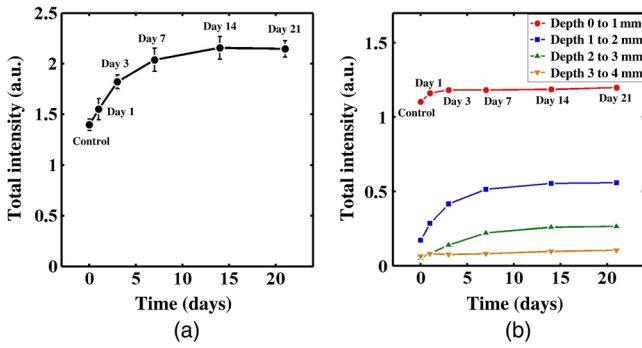


Fig. 7 Intensity analysis of the decalcified guinea pig cochlea OCT images: (a) the averaged intensity in the depth direction on each imaging day and (b) the total intensity with respect to the depth range as a function of imaging days.

pig cochlea samples. As a result of the sample size difference, a gradual improvement of the intensity was clearly observed.

As described above, we repeated the quantitative analysis for further numerical calculation. In our calculation, the averaged intensity of the control sample was 1.40 ± 0.06 and the maximal intensity (on the 14th day) was 2.12 ± 0.11 . Therefore, an intensity increase of 54.3% compared to the control sample can be observed on the 14th day. Similar calculation was performed on each experimental day by comparing the intensity variation with respect to that for the control stage. The calculated values increased by 11.0, 30.3, 45.8, 54.3, and 53.7% on the 1st, 3rd, 7th, 14th, and 21st days, respectively. The results confirm

that the maximal intensity was observed on the 14th day, and further, the total intensity on the following days is saturated. Hence, it was revealed that the most optimal duration of decalcification of the guinea pig cochlea was 14 days using the acquisition of the image with the point of the intensity saturation.

The similar experiment was performed to verify the efficacy of the EDTA-based optical clearing method further and to confirm the enhancement of the depth intensity precisely. The results are shown in Fig. 7(b). A noticeable intensity fluctuation was not observed in the depth range of 0 to 1 mm. However, an identifiable intensity fluctuation was observed in the depth range of 2 to 4 mm. Owing to the effects of EDTA-based decalcification, results similar to Fig. 7(a) were obtained as the maximal intensity was observed on the 14th day as expected, and the total intensity on the following days was saturated.

The intensity fluctuation of each depth range shown in Fig. 7(b) was calculated by analyzing the intensity variation with respect to that for the control stage on each experimental day. Therefore, variations of 5.4, 7.2, 7.3, 7.6, and 8.7% within the depth range of 0 to 1 mm were observed on the 1st, 3rd, 7th, 14th, and 21st days, respectively. The intensity variations within the depth range of 1 to 2 mm were 65.6, 142.2, 198.4, 221.8, and 224.3 on the 1st, 3rd, 7th, 14th, and 21st days, respectively. The intensity increased by 221.8% on the 14th day compared to that for the control stage. In the depth range of 2 to 3 mm, the intensity increased by 418.2% on the 14th day compared to that for the control stage and became saturated within 2.8%. In the depth range of 3 to 4 mm, intensity fluctuations of 23.5, 15.2, 25.2,

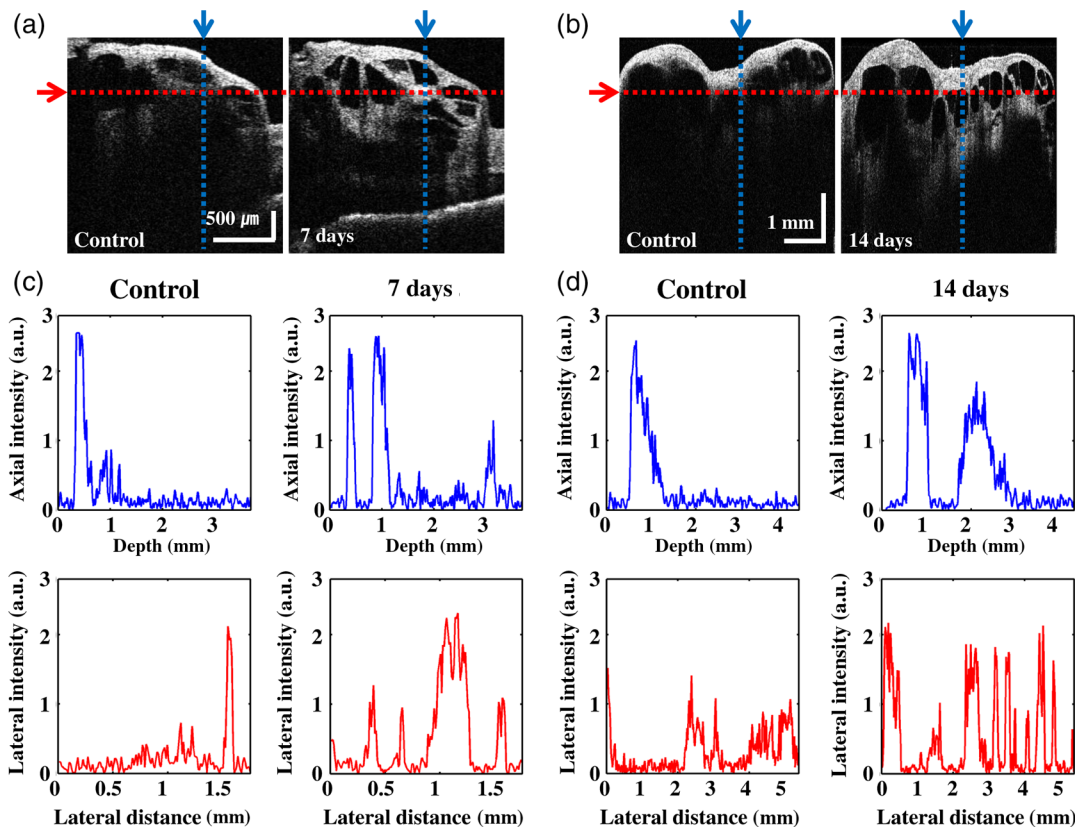


Fig. 8 A-scan analysis of the obtained images in the axial and lateral directions: (a) the calculated 2-D control sample image and the image of the mouse cochlea obtained on the 7th day, (b) the calculated 2-D control sample image and the image of the guinea pig cochlea obtained on the 14th day, and (c) and (d) the results of the A-scan analysis of the 2-D images obtained in the axial and lateral directions.

47.5, and 60.5% were observed on the 1st, 3rd, 7th, 14th, and 21st days, respectively, confirming the effectiveness of the proposed decalcification method. The calculated average intensity within the depth range of 0 to 1 mm was 1.17, and the average intensity within the depth range of 3 to 4 mm was 0.08. Therefore, the effect of decalcification is negligible in the depth range of 3 to 4 mm compared with that in the depth range of 0 to 1 mm.

Additionally, we evaluated both the mouse and guinea pig cochlea microstructures in the axial and lateral directions through an A-scan analysis. The enhancement of the depth visibility, owing to optical clearing, was calculated by comparing the A-scans of the control sample image and the image whose intensity is maximal (mouse: 7th day and guinea pig: 14th day). Figures 8(a) and 8(b) depict the calculated mouse and guinea pig control sample 2-D images along with the images whose intensities are maximal. The blue and red lines in the axial and lateral directions represent the specific region for the A-scan analysis. The graphs plotted in blue color represent the axial direction A-scans, and the graphs plotted in red color represent the lateral direction A-scans [Figs. 8(c) and 8(d)]. A clear correlation between the 2-D images and the calculated A-scans can be revealed. The blue color A-scans shown in Figs. 8(c) and 8(d) were extracted along the blue vertical dashed lines in Figs. 8(a) and 8(b). From these A-scans, the increase of the image intensity as well as the gradual depth visibility enhancement was verified through the appearance of the peaks. Furthermore, the red color A-scans shown in Figs. 8(c) and 8(d) were extracted along the red-colored horizontal dashed lines in Figs. 8(a) and 8(b). Similarly, from the A-scans, the increase of the image intensity as well as the clear visualization of the bony walls in the horizontal direction can be confirmed through the appearance of the distinguishable peaks. Crucial structural information can be obtained from the lateral direction A-scans compared to the depth direction A-scans. According to the results, a clear difference can be observed in both axial and lateral direction A-scans of the mouse cochlea (7th day) and guinea pig cochlea (14th day) samples compared to the respective control samples, owing to the effect of decalcification. Therefore, A-scan calculation confirms the rigorous optical clearing effectiveness using the clear A-scan peaks, which represent the internal microstructures verifying the enhanced depth visibility compared to that of the control samples.

4 Conclusions

We implemented a decalcification-based optical clearing effect to mouse and guinea pig cochlea samples to enhance the depth visualization of internal microstructures using OCT. The obtained 2-D OCT images successfully illustrated the feasibility of the proposed method by providing clearly visible microstructures in the depth direction as a result of decalcification. The effectiveness of decalcification of the mouse cochlea was observed on the first experimental day, and the best results were observed after seven days owing to the sample size. However, the most optimal clearing results for the guinea pig cochlea were obtained after 14 consecutive days. Moreover, the necessity of histological sectioning methods could be minimized owing to the clear visibility of bony cochlear turns at the entire depth sections. The quantitative assessment results verify the increase of the intensity as well as the thickness measurements of the internal microstructures. Therefore, the proposed

EDTA-based optical clearing method can be considered as a potential application for depth-enhanced OCT visualization.

Acknowledgments

We express our deepest thanks to Professor Jeehyun Kim of Kyungpook National University for his continuous help and support. Also, we thank Professor Jaewon Song of Kyungpook National University who did the guidance of experiment and the written part of the manuscript. And, the authors are grateful to the Industrial Strategic Technology Development Program, Grant No. 10047943; the Development of Microsurgical Apparatus based on 3D Tomographic Operating Microscope program, funded by the Ministry of Trade, Industry & Energy (MI, Korea, No. 10047943). This study was also supported by BK21 Plus project funded by the Ministry of Education, Korea (21A20131600011), and this research was conducted under the industrial infrastructure program of laser industry support, which is funded by the Ministry of Trade, Industry & Energy, Korea (N0000598).

References

1. B. A. Ghaheri et al., "Cochlear cytokine gene expression in murine chronic otitis media," *Otolaryngol. Head Neck Surg.* **137**(2), 332–337 (2007).
2. W. Würfel et al., "Cochlear length determination in temporal bone specimens using histological serial micro grinding imaging, micro computed tomography and flat-panel volumetric computed tomography," *Online J. Otolaryngol.* **5**(2), 39–59 (2015).
3. Y. Liu et al., "Effects of a dexamethasone-releasing implant on cochlea: a functional, morphological and pharmacokinetic study," *Hear. Res.* **327**, 89–101 (2015).
4. S. A. Counter et al., "Experimental fusion of contrast enhanced high-field magnetic resonance imaging and high-resolution micro-computed tomography in imaging the mouse inner ear," *Open Neuroimaging J.* **9**, 7 (2015).
5. H. Yamazaki et al., "Usefulness of MRI and EABR testing for predicting CI outcomes immediately after cochlear implantation in cases with cochlear nerve deficiency," *Otol. Neurotol.* **36**(6), 977–984 (2015).
6. J. A. Izatt et al., "Micrometer-scale resolution imaging of the anterior eye in vivo with optical coherence tomography," *Arch. Ophthalmol.* **112**(12), 1584–1589 (1994).
7. J. Welzel, "Optical coherence tomography in dermatology: a review," *Skin Res. Technol.* **7**(1), 1–9 (2001).
8. D. Huang et al., "Optical coherence tomography," *Science* **254**(5035), 1178–1181 (1991).
9. M. Jeon et al., "Full-range k-domain linearization in spectral-domain optical coherence tomography," *Appl. Opt.* **50**(8), 1158–1163 (2011).
10. W. Jung et al., "Handheld optical coherence tomography scanner for primary care diagnostics," *IEEE Trans. Biomed. Eng.* **58**(3), 741–744 (2011).
11. J. Kim, B.-S. Sohn, and T. E. Milner, "Real-time retinal imaging with a parallel OCT using a CMOS smart array detector," *J. Korean Phys. Soc.* **51**(5), 1787–1791 (2007).
12. N. H. Cho et al., "Evaluation of the usefulness of three-dimensional optical coherence tomography in a guinea pig model of endolymphatic hydrops induced by surgical obliteration of the endolymphatic duct," *J. Biomed. Opt.* **20**(3), 036009 (2015).
13. S. S. Gao et al., "Quantitative imaging of cochlear soft tissues in wild-type and hearing-impaired transgenic mice by spectral domain optical coherence tomography," *Opt. Express* **19**(16), 15415–15428 (2011).
14. H. Wilhelm Pau et al., "Optical coherence tomography as an orientation guide in cochlear implant surgery?," *Acta Oto-Laryngol.* **127**(9), 907–913 (2007).
15. B. J. Wong et al., "Imaging the internal structure of the rat cochlea using optical coherence tomography at 0.827 μm and 1.3 μm ," *Otolaryngol. Head Neck Surg.* **130**(3), 334–338 (2004).
16. J. Lin, H. Staecker, and M. S. Jafri, "Optical coherence tomography imaging of the inner ear: a feasibility study with implications for

- cochlear implantation," *Ann. Otol., Rhinol., Laryngol.* **117**(5), 341–346 (2008).
17. A. Sepehr et al., "Optical coherence tomography of the cochlea in the porcine model," *Laryngoscope* **118**(8), 1449–1451 (2008).
 18. H. M. Subhash et al., "Volumetric in vivo imaging of intracochlear microstructures in mice by high-speed spectral domain optical coherence tomography," *J. Biomed. Opt.* **15**(3), 036024 (2010).
 19. N. H. Cho et al., "In vivo imaging of middle-ear and inner-ear microstructures of a mouse guided by SD-OCT combined with a surgical microscope," *Opt. Express* **22**(8), 8985–8995 (2014).
 20. V. V. Tuchin, *Optical Clearing of Tissues and Blood*, SPIE Press, Bellingham (2006).
 21. D. Zhu et al., "Recent progress in tissue optical clearing," *Laser Photonics Rev.* **7**(5), 732–757 (2013).
 22. K. V. Larin et al., "Optical clearing for OCT image enhancement and in-depth monitoring of molecular diffusion," *IEEE J. Sel. Topics Quantum Electron.* **18**(3), 1244–1259 (2012).
 23. J. Zhou and S. Shore, "Projections from the trigeminal nuclear complex to the cochlear nuclei: a retrograde and anterograde tracing study in the guinea pig," *J. Neurosci. Res.* **78**(6), 901–907 (2004).
 24. D. S. Richardson and J. W. Lichtman, "Clarifying tissue clearing," *Cell* **162**(2), 246–257 (2015).

Mansik Jeon received his PhD in electrical engineering from Kyungpook National University, Daegu, Republic of Korea, in 2011. He is currently an assistant professor of School of Electronics Engineering at Kyungpook National University. His research interests are in the development of nonionizing and noninvasive novel biomedical imaging techniques, including photoacoustic tomography, optical coherence tomography, ultrasonic imaging, handheld scanner, and their clinical applications.

Biographies for the others authors are not available.